

See discussions, stats, and author profiles for this publication at: <https://www.researchgate.net/publication/381301289>

Self-Calibration of the Horus All-Digital Phased Array Using Mutual Coupling

Conference Paper · May 2024

DOI: 10.1109/RadarConf2458775.2024.10548360

CITATIONS

5

READS

254

4 authors, including:



[Matthew Herndon](#)

University of Oklahoma

13 PUBLICATIONS 130 CITATIONS

[SEE PROFILE](#)







[David Schwartzman](#)

University of Oklahoma

96 PUBLICATIONS 564 CITATIONS

[SEE PROFILE](#)

Self-Calibration of the Horus All-Digital Phased Array using Mutual Coupling

Matthew Herndon¹, David Schwartzman^{1,2,3}, Caleb Fulton^{1,2}, Mark Yeary^{1,2}

¹Advanced Radar Research Center (ARRC)

²School of Electrical and Computer Engineering

³School of Meteorology

The University of Oklahoma, Norman, OK, USA

Email: mherndon@ou.edu, dschvart@ou.edu, fulton@ou.edu, yeary@ou.edu

Abstract—Calibration of digital phased array radars is of crucial importance for future radar surveillance systems, especially for high-accuracy polarimetric measurements needed for weather observations. Mutual coupling calibration (or self-calibration) leverages the coupling between antenna elements to derive alignment weights, and can be applied both at system start-up and in real-time during operations to initialize and maintain radar calibration. An operational implementation of mutual coupling calibration has been developed to calibrate the fully digital Horus radar system, and has now been fielded many times to support a variety of data collection experiments. This paper discusses our implementation and summarizes results from several experiments aimed at assessing calibration quality. Our results confirm the efficacy of the methods through ground-truth experiments at different array scales. It also validates beamforming post-calibration through precise far-field patterns measured from an uncrewed aerial system (UAS) which strongly agree with simulated patterns to within ± 0.15 dB at boresight. We believe that this is the first demonstration of holistic experiments assessing mutual coupling calibration performance in a large digital array.

Index Terms—PAR, Calibration, Mutual Coupling, Digital Array, UAS, Far-field

I. INTRODUCTION

Phased array antennas have inherent elemental S-parameters that are largely self-similar throughout antenna elements in the array. This feature holds true across the array, except near the edges. Moreover, these S-parameters are stable over time and temperature, assuming no antenna hardware failures or broken connections. In all-digital arrays, each antenna port is connected to a digital transceiver, enabling precise measurement of mutual couplings between elements. These “couplings” are measured by transmitting from a single element and receiving on one or many others (see Fig. 1 for diagram), then estimating a complex, effective “coupling” for each path. Measuring couplings from all transmitters to all receivers provides a complete picture of the array’s coupling state which is useful for alignment calibration purposes. Given the stability of the couplings themselves, the dominant source of array error may be assumed to be from the transceivers and front-end hardware rather than array antennas (assuming few physically- or electrically- broken elements). Following from this assumption, array errors can be reliably estimated

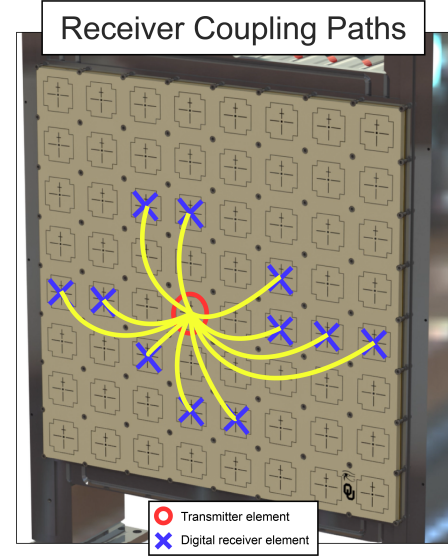


Fig. 1: Approximate coupling paths from a single transmitter to an arbitrary set of receivers on a single Horus 8×8 all-digital panel.

by comparing couplings. Our team’s reference-based mutual coupling calibration follows from this assumption and aims to estimate alignment differences between an array in its current state and a reference state—measured after calibration by another method. This method has been extensively studied by our group [1], [2], and an implementation has been developed and matured for use in calibrating large Horus all-digital radar systems. Horus is an S-band, digital-at-every-element polarimetric phased array radar under development at the University of Oklahoma [3], [4], [5]. Several Horus systems are under active development—one is known as Horus-NOAA, and another is called Horus-DoD. This conference paper discusses recent research activities which were conducted using Horus-NOAA, which has been operational since 2022. Both radars were designed and are being built at the University of Oklahoma’s Advanced Radar Research Center (ARRC). The radar employs a tileable architecture, with each tile containing 8×8 elements as shown in Fig. 1. At its core, reference based mutual coupling calibration provides a mechanism to

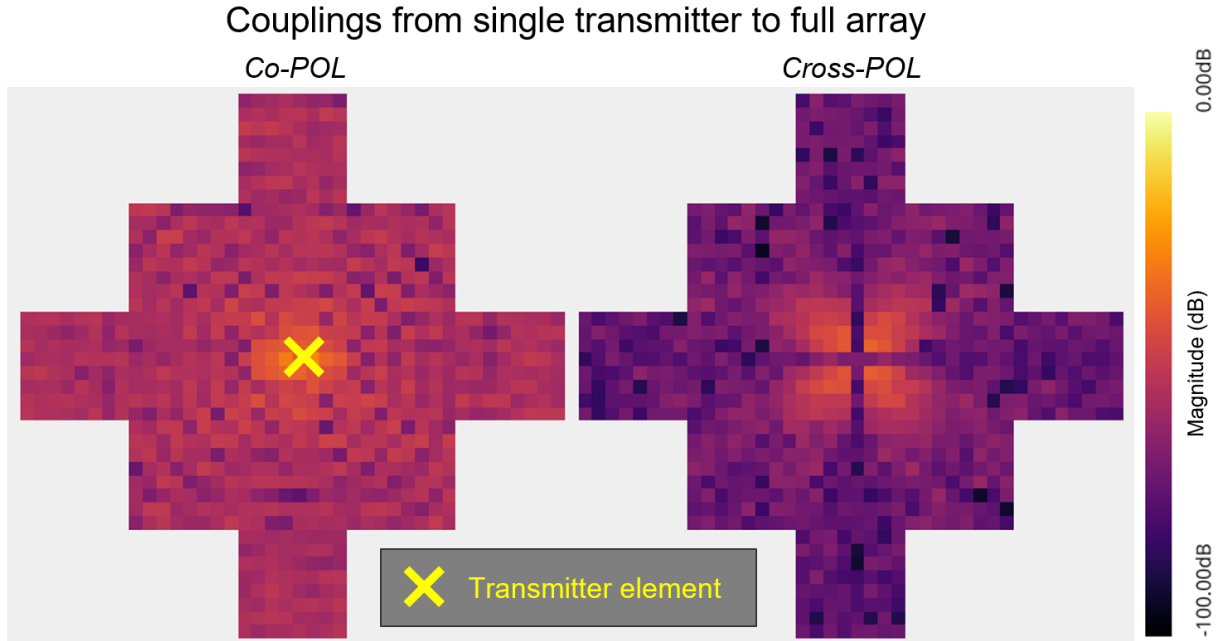


Fig. 2: A single coupling measurement from a 13-panel, dual-pol, 1664-element array. During mutual coupling calibration, every transmitter produces a similar measurement.

align phased arrays in the field using self-measured couplings. In this paper, we discuss our implementation of this method including our algorithm, measurement details unique to digital array technology, and several critical optimizations required to make the process practical. We provide examples of the method as applied to modular Horus systems in a variety of configurations showing the method’s scale-ability and robustness. Lastly, we present farfield measurements of the Horus-NOAA 13-panel antenna patterns, collected after calibration using this method. Results demonstrate precise alignment across the array, and thereby provide support for the effectiveness of reference-based mutual coupling calibration in an operational setting.

II. REFERENCE-BASED MUTUAL COUPLING CALIBRATION IN HORUS

Reference-based mutual coupling calibration is used to estimate alignment offsets between an array in its current state and those established during a reference, or “gold standard” state, previously captured with the array in some desired configuration in a controlled environment (e.g. a near-field chamber), [6]. Our group has developed a reference-based mutual coupling calibration algorithm which is used operationally to calibrate Horus digital radar systems. At a high-level, our implementation has evolved from what is documented in [2], [7], [8], [9], [10], and is summarized in the next section. With all of this in mind, we state: differing from others, and for the first time, we demonstrate these concepts with actual measurements on a large-scale digital-at-every-element array.

A. Coupling measurements in Horus

To begin, a reference coupling matrix is captured with the array in a desired configuration, such as after alignment using

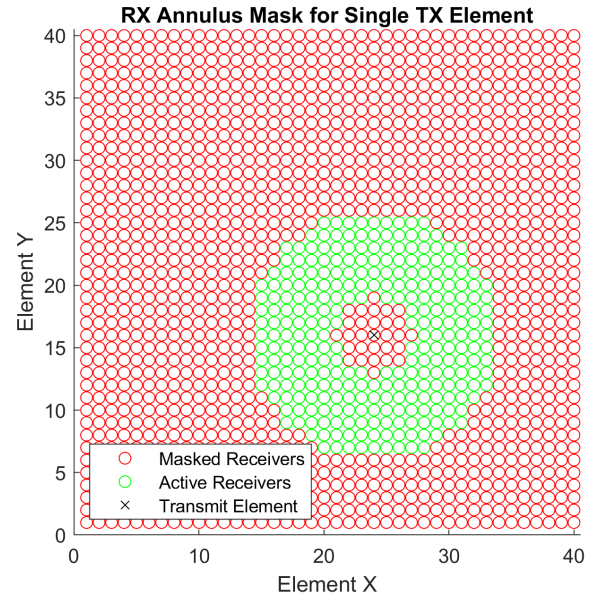


Fig. 3: Visualization of the couplings selected when using an annulus mask.

standard nearfield (NF) or farfield (FF) alignment calibration procedures. In the Horus fully digital architecture, every single element within the array can be individually excited on transmit then observed from an arbitrary number of receiver elements. Each receiver measures baseband I/Q of a signal coupled from the transmitter, which is then used to compute a complex phasor encoding the magnitude, phase, and SNR estimate for the measurement. The coupling is measured from the IQ using FFT-based methods, and SNR is derived from the relative strength of out-of-band frequency components

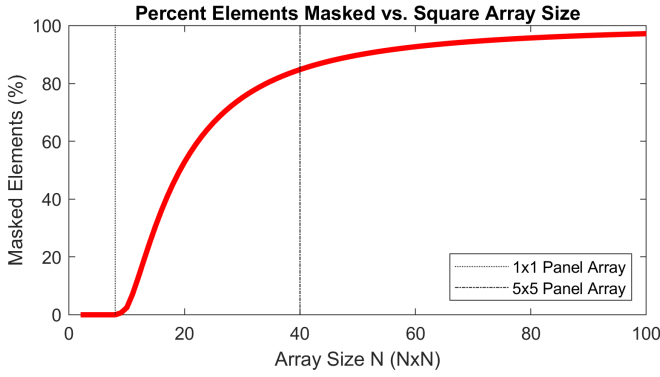


Fig. 4: Total reduction (in percentage of total uncensored pulses) in pulses when using annulus masking vs. square array size, highlighting existing array sizes.

compared to in-band. Fig. 2 shows the magnitude (in dBFS) of the couplings from a single transmitter to all receivers the 13-panel Horus-NOAA demonstrator. Repeating this pattern and transmitting at least once from all elements provides information about every element-to-element coupling in the array. The following steps detail how coupling measurements are captured and organized for use in the final algorithm:

- 1) Sequentially transmit on each element, simultaneously receiving on all other elements while storing data from groups of elements that are associated with each transmit element,
- 2) Through windowing and FFT-based estimates at a given frequency bin, determine the effective complex couplings represented by each of these measurements,
- 3) Express the resulting couplings in matrix form as \mathbf{TR} , with the row corresponding to the Rx element index and column to the Tx element.

In practice, measuring and processing large numbers of coupling pairs requires substantial compute and memory resources, all-the-while adding to the overall latency of the calibration process. One critical optimization to reduce the number of measurements required for mutual coupling is to pre-select which receivers should be active for each transmitter. In Horus, several rules are used as selection criteria ahead-of-time based purely on array geometry. Coupling strength on the array's 2D surface rapidly falls off as a function of distance r^2 from the transmit element, so in practice couplings further than some distance r_{max} from the transmitter can be ignored without penalty. Alternately, receivers close to the transmitter are likely to be saturated, rendering their measurement unusable. Therefore, masking away elements closer than r_{min} preemptively censors most of these problematic measurements. Selecting for the region $r_{min} < x < r_{max}$ produces the combination mask, seen in Fig. 3 (with arbitrary selection parameters). In both cases, the masks may either exclude useful couplings or fail to exclude problematic couplings, but in general provide a useful heuristic for reducing the information burden of mutual coupling measurements. an effect which grows rapidly with array scale (see Fig. 4).

B. Calibration in the Field

For a given reference coupling matrix and the array in some new unknown state (e.g. after temperature changes, aging, power cycling, etc.), reference-based mutual coupling calibration is used to achieve alignment following these steps:

- 1) Repeat the coupling measurements described in Section II-A, store in matrix form as \mathbf{TR}' ,
- 2) Estimate the errors (changes to Tx and Rx responses on each channel) by making mutual coupling measurements. The Tx and Rx errors are stacked as vector \mathbf{E} of size $2N \times 1$ for an N -element array.
 - a) Compute the matrix $\mathbf{C} = \log(\mathbf{TR}' \oslash \mathbf{TR})$, with \oslash being the inverse Hadamard product (or, more simply, element-wise division).
 - b) Construct a vector \mathbf{M} consisting of “stacked” non-zero entries of \mathbf{C} .
 - c) Construct a matrix \mathbf{A} by appending a 0's row with 1's placed at the indices of the transmitter and receiver for each entry in \mathbf{C} ,
 - d) Select an element to act as a “reference” in terms of amplitude and phase, typically a receiver whose average response to each transmitter is “close” to that which was measured in the golden standard (this is one of many approaches to this particular step). Construct the matrix \mathbf{D} , which is the identity matrix except with a 0 in the diagonal entry associated with the reference element.
 - e) Estimate the transmit and receive errors using the Moore-Penrose pseudoinverse (denoted here with the \dagger operator) to find a least-square fit for the solution: $\mathbf{E} = e^{(\mathbf{CD})^\dagger \mathbf{M}/N}$. Note that the logarithm made previously is being inverted, here, to turn to “standard” complex error terms.
- 3) Finally, apply digital weights representing the inverses of the complex errors in \mathbf{E} on each transmitter and each receiver, aligning the array.

III. RESULTS

A. Ground-truth Experiments

While engaging in efforts to improve our mutual coupling methods, an experiment was designed to measure the relative performance of reference-based mutual coupling quickly which enabled faster iteration while investigating and developing algorithm improvements. A calibration horn was placed 2 m in front of the array and connected to an optical delay line (ODL) repeater. Next, an element on a target array in front of the calibration horn was selected as a reference, which serves as either a transmitter or receiver depending on the desired calibration mode (TX or RX). For the RX case, the reference element transmits towards the calibration horn and has its excitation re-radiated towards the array face after a time delay, which is then received by all elements in the array. The TX case inverts this topology, with the reference element receiving returns from each transmit element re-radiated by the ODL. For both cases, the element-level returns from the

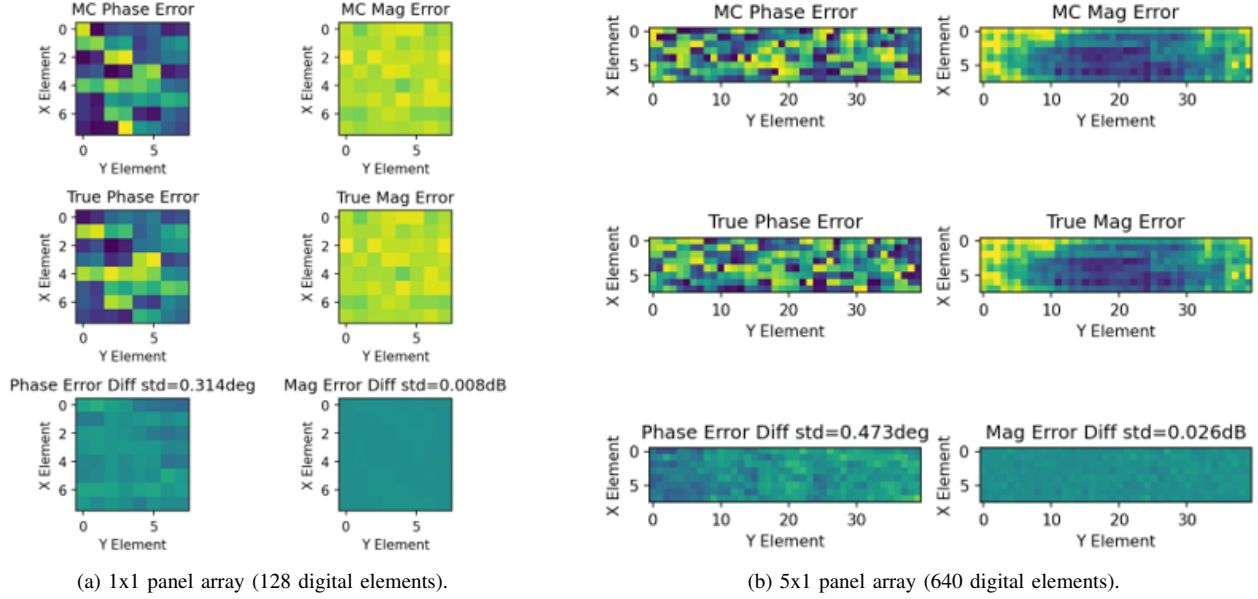


Fig. 5: Comparison between ground truth array errors and the error estimates produced by our reference-based mutual coupling method at different array sizes. Figures show receive mode estimates.

measurement allowed were used to compute alignment weights which effectively focused the array onto a repeatable point in space. Although the resultant array alignment state served no operational purpose, the experiment established a reproducible array state with measurable ground-truth.

With the array focused to the nearfield, these ideal alignment weights were saved off as the *true* errors and mutual coupling reference was measured to serve as the target array state for mutual coupling calibration. Next, the array was returned to its initial uncalibrated state, simulating operational startup. From this state, mutual coupling calibration was applied targeting the calibration reference captured previously. Lastly, the results from mutual coupling calibration were compared against the ground truth weights. The standard deviation of the difference between the ground truth errors and the mutual coupling error estimates providing a fitness metric to minimize while working to improve the mutual coupling solver.

Fig. 5 shows two sets of results from these experiments for two different array sizes. These plots show the mutual coupling error estimates (top), the ground truth array errors (middle), and the difference between the two results (bottom). Additionally, the standard deviation of the difference (separate for phase and magnitude) is included, as this served as an important fitness metric we sought to minimize while improving mutual coupling solution finding. At both scales, our method produces high-quality error estimates which strongly agree with the ground truth errors, demonstrating the scale-ability of our method.

B. Far-field Antenna Pattern Measurements

We deployed the Horus radar in the parking lot of OU's Lloyd Noble Center and conducted experiments aimed at measuring the two-dimensional radiation patterns. A newly

developed uncrewed aerial systems (UAS) system, the “RF-Sonde”, was used to measure the radiation patterns in the far-field [11], [12]. For the experiment, the radar was parked facing south to the Jim Traw Field, a field dedicated to flying remote controlled UAS. The Horus antenna was mechanically positioned at 45° in elevation, to avoid contamination from multi-path returns or external interference as shown in Fig. 6. Prior to starting the antenna pattern measurements, the Horus radar initiated the mutual-coupling calibration routine.

Co-polar H antenna patterns are presented in Figure 7, where the left panel shows a simulated Horus copolar H antenna pattern, and the middle panel shows the measured copolar H antenna pattern. The dotted black contour lines overlaid represent the half-power beamwidth (-3 dB from the peak). On the right panel, power differences between the simulated and measured pattern mainlobes are presented (data are from the peak down to the -10 dB power level). We evaluate the performance of mutual coupling calibration by comparing far-field measurements to simulated Horus array patterns. For the simulation, a hybrid approach is used, whereby the copolar embedded element pattern is multiplied by the array factor to set the correct gain roll-off [13]. Amplitude and phase excitation errors are introduced in the simulated patterns, and the average copolar pattern differences from the peak (normalized to 0 dB) down to -20 dB are computed between the ideal simulation (i.e., no errors) and those with excitation errors. These errors are systematically simulated for each element independently using zero-mean Gaussian distributions. For the magnitude, fluctuations with standard deviation (STD) from 0 to 1 dB in steps of 0.01 dB are added to the excitations to simulate calibration errors. A similar procedure is carried out for the phase errors, from 0° to 10° in steps of 0.1° . The

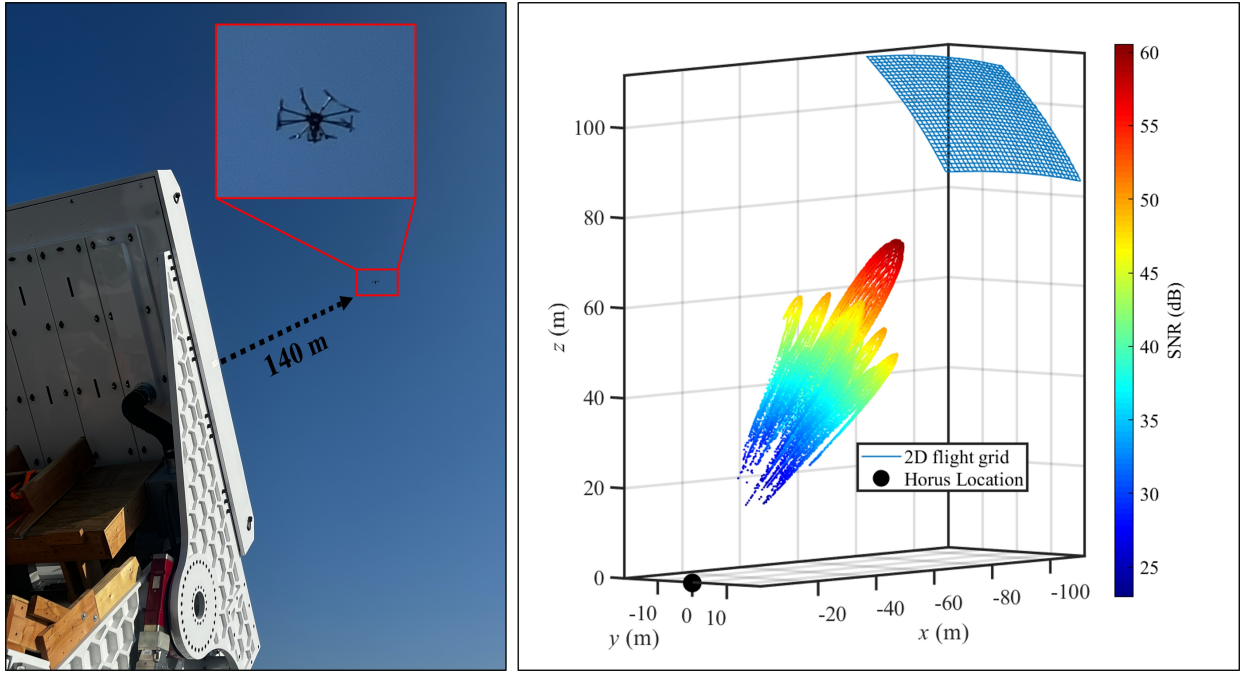


Fig. 6: Far-field measurements of the Horus system's transmit beam after mutual coupling calibration. The left panel shows the UAS scanning the Horus antenna pattern in the far field (>140 m range). Three-dimensional plot illustrating the flight grid traversed by the UAS, depicted relative to the position of the Horus radar (black dot on the right panel).

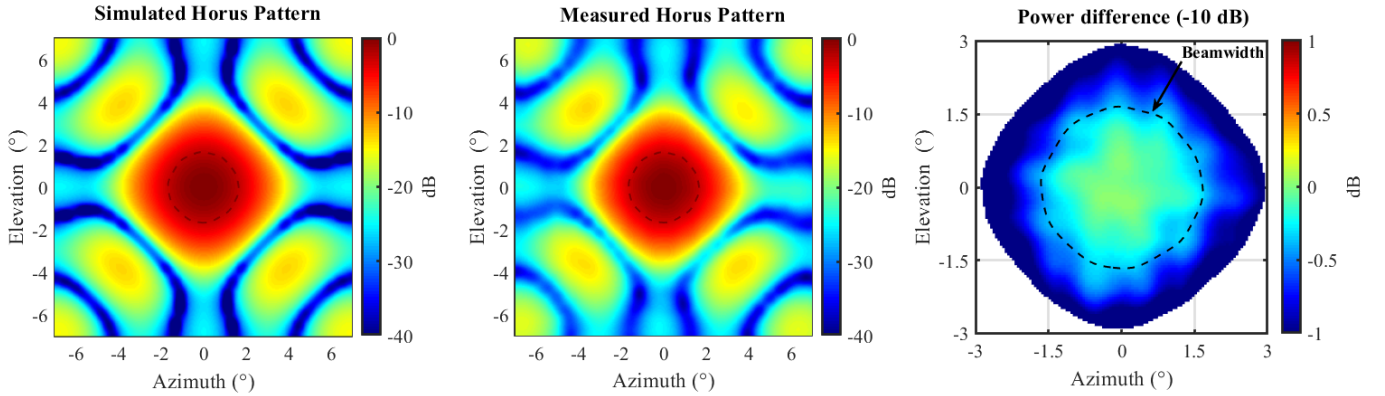


Fig. 7: Two-dimensional co-polar H antenna far-field patterns measured with a UAS. The left and middle panels show simulated and measured Horus co-polar H antenna patterns, and the right panel shows the power difference between these patterns.

resulting average copolar differences between simulated far-field patterns are presented in Fig. 8. The contour plot indicates estimated mean difference between the far-field UAS-based Horus pattern measurement and the ideal pattern.

IV. CONCLUSION

This paper discusses an implementation of reference-based mutual coupling calibration developed for operational calibration of Horus digital array systems. We discuss our algorithm in an abstract sense, including one important optimization to the measurement process with implications for larger arrays. Following this, we detail the results of ground-truth experiments which validate the performance of our method across array scales. Lastly, we present farfield measurements

of the Horus-NOAA 13-panel system after calibration using our methods. Overall, these results provide strong support for our method's effectiveness at estimating array alignment errors in the field, enabling precise beamforming.

V. ACKNOWLEDGEMENT

This work is supported primarily by NOAA/Office of Oceanic and Atmospheric Research under NOAA-University of Oklahoma Cooperative Agreement #NA21OAR4320204, U.S. Department of Commerce. It is also partially supported from the U. S. Office of Naval Research under award numbers N00014-19-1-2326 and N00014-20-1-2851. Special thanks to the ARRC's engineering staff for their dedication to the project.

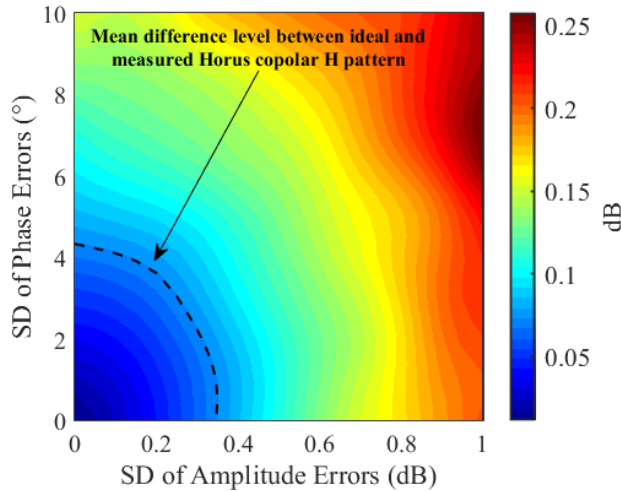


Fig. 8: Average copolar pattern differences from the peak (normalized to 0 dB) down to -20 dB between the ideal simulation (i.e., no errors) and those simulated with excitation errors. The contour plot indicates estimated mean difference between the far-field UAS-based Horus pattern measurement and the ideal pattern.

REFERENCES

- [1] C. Fulton, P. Kenworthy, J. Lujan, M. Herndon, S. Garner, D. Thompson, and M. Yeary, "Mutual coupling-based calibration for the horus digital phased array radar," in *2022 IEEE International Symposium on Phased Array Systems & Technology (PAST)*, 2022, pp. 1–6.
- [2] C. Fulton, J. L. Salazar, Y. Zhang, G. Zhang, R. Kelly, J. Meier, M. McCord, D. Schmidt, A. D. Byrd, L. M. Bhowmik, S. Karimkashi, D. S. Zrnic, R. J. Doviak, A. Zahrai, M. Yeary, and R. D. Palmer, "Cylindrical polarimetric phased array radar: Beamforming and calibration for weather applications," *IEEE Transactions on Geoscience and Remote Sensing*, vol. 55, no. 5, pp. 2827–2841, 2017.
- [3] R. D. Palmer, M. B. Yeary, D. Schwartzman, J. L. Salazar-Cerreno, C. Fulton, M. McCord, B. Cheong, D. Bodine, P. Kirstetter, H. H. Sigmarsson *et al.*, "Horus—a fully digital polarimetric phased array radar for next-generation weather observations," *IEEE Transactions on Radar Systems*, 2023.
- [4] M. Yeary, R. Palmer, C. Fulton, J. Salazar, and H. Sigmarsson, "Update on an S-band all-digital mobile phased array radar," in *2021 IEEE Radar Conference (RadarConf21)*. IEEE, 2021, pp. 1–4.
- [5] C. Fulton, N. Goodman, M. Yeary, R. Palmer, H. Sigmarsson, and J. McDaniel, "Preliminary system integration and performance features for an S-band, dual-polarized, all-digital phased array radar," in *2022 IEEE/MTT-S International Microwave Symposium-IMS 2022*. IEEE, 2022, pp. 862–864.
- [6] D. Schwartzman, J. D. D. Díaz, D. Zrnić, M. Herndon, M. B. Yeary, and R. D. Palmer, "Holographic back-projection method for calibration of fully digital polarimetric phased array radar," *IEEE Transactions on Radar Systems*, vol. 1, pp. 295–307, 2023.
- [7] C. Fulton and W. J. Chappell, "Calibration of a digital phased array for polarimetric radar," in *Microwave Symposium Digest (MTT), 2010 IEEE MTT-S International*. IEEE, 2010, pp. 161–164.
- [8] D. Bekers, R. van Dijk, and F. van Vliet, "Mutual-coupling based phased-array calibration: A robust and versatile approach," in *2013 IEEE International Symposium on Phased Array Systems and Technology*, 2013, pp. 630–637.
- [9] A. E. Mitchell, "Coupling-based wideband digital phased array calibration techniques," Master's thesis, The University of Oklahoma, 2013.
- [10] C. Fulton, G. Zhang, W. Bocangel, L. Lei, R. Kelley, and M. McCord, "Cylindrical polarimetric phased array radar: A multi-function demonstrator and its calibration," in *Microwaves, Communications, Antennas and Electronics Systems (COMCAS), 2013 IEEE International Conference on*, 2013, pp. 1–5.
- [11] A. Segales *et al.*, "Uas-based antenna pattern measurements of the fully digital horus phased array radar," in *2024 IEEE Radar Conference (RadarConf24)*, 2024, pp. 01–06.
- [12] A. R. Segales, D. Schwartzman, K. Burdi, J. Salazar-Cerreno, C. Fulton, and R. Palmer, "Far-field antenna pattern measurements using a uas-based dynamic gimbal scan system," *IEEE Transactions on Antennas and Propagation*. Under Review., 2023.
- [13] D. Schwartzman, J. D. D. Díaz, J. L. Salazar-Cerreño, T.-Y. Yu, R. D. Palmer, and M. S. McCord, "A hybrid antenna pattern synthesis method for the polarimetric atmospheric imaging radar (pair)," in *2022 IEEE Radar Conference (RadarConf22)*, 2022, pp. 01–06.